Accurate estimation of evolutionary power spectra for strongly narrow-band random fields

Dominik Schillinger [a,*], Vissarion Papadopoulos [b]

[a] Chair for Computation in Engineering, Department of Civil Engineering and Surveying, Technische Universität München, Arcisstr. 21, 80333 München, Germany
[b] Institute of Structural Analysis and Seismic Research, National Technical University of Athens, 9 Iroon Polytechneiou, Zografou Campus, Athens 15780, Greece

ARTICLE INFO

ABSTRACT

One of the most widely used techniques for the simulation of non-homogeneous random fields is the spectral representation method. Its key quantity is the power spectrum, which characterizes the random field in terms of frequency content and spatial evolution in a mean square sense. The paper at hand proposes a method for the estimation of separable power spectra from a series of samples, which combines accurate spectrum resolution in space with an optimum localization in frequency. For non-separable power spectra, it can be complemented by a joint strategy, which is based on the partitioning of the space-frequency domain into several sub-spectra that have to be separable only within themselves. Characteristics and accuracy of the proposed method are demonstrated for analytical benchmark spectra, whose estimates are compared to corresponding results of established techniques based on the short-time Fourier, the harmonic wavelet and the Wigner–Ville transforms. It is then shown by a practical example from stochastic imperfection modeling in structures that in the presence of strong narrow-bandedness in frequency, the proposed method for separable random fields leads to a considerable improvement of estimation results in comparison to the established techniques.

© 2009 Elsevier B.V. All rights reserved.

1. Introduction

Within the last three decades, computational stochastic mechanics has evolved into a self-contained and prolific field of research, which has brought forth a wide range of sophisticated and well-established methodologies for the stochastic simulation of uncertain engineering systems [6,8,33,40,42]. Due to the rapidly growing availability of large-scale and cheap computer power, the intensive computational demands of these techniques become more and more manageable today, which makes stochastic simulation increasingly interesting for actual use in engineering practice. One emerging field of application is the stability analysis of thin-walled structures [7,40], where the random variability of geometric and material imperfections leads to considerable uncertainty in corresponding buckling loads. As a starting point, a series of computational studies has recently shown that the influence of random imperfections on the size and variability of the ultimate strength of cylindrical shells can be reproduced with respect to corresponding experimental tests [1,23–26,32–34,38].

Apart from algorithmic maturity, the quality of stochastic simulation methods predominantly depends on the accurate reproduction of the random physical key phenomena by corresponding random field models. In the case of imperfection triggered buckling, a small misrepresentation of the physical imperfection wave length in the imperfection model can lead to a large discrepancy between real and simulated system response, because the dominant buckling mode might shift to a higher Eigenform, leading to an unphysical increase in ultimate strength. One of the most widely used techniques for the simulation of imperfections as random fields is the spectral representation method [9,35,36,39]. The key quantity of spectral representation is the power spectrum [18,27,28,30,31,44], which is related to the average energy of the random field and is obtained for example in earthquake applications by estimation from measured ground motion accelerations [4,12,37]. Despite its decisive importance for realistic stochastic buckling simulations, only little experience exists so far in transferring experimental imperfection measurements, which typically are strongly narrow-band functions at very low frequencies, into accurate evolutionary power spectra. Up to now, measurement based evolutionary imperfection modeling relies on the adoption of established time–frequency analysis techniques from digital time signal processing [24,25].

Against this background, the present paper intends to shed some light on key issues related to the evolutionary power spectrum estimation of strongly narrow-band random fields, with special emphasis on their application to imperfection modeling in structures. First, a concise review of existing methods for the estimation of evolutionary power spectra [2,3,27] is presented. Second, a simple yet effective method for evolutionary spectrum

---

* Corresponding author. Tel.: +49 89 289 25116; fax: +49 89 289 25051.
E-mail address: schillinger@bv.tum.de (D. Schillinger).

estimation of separable random fields is introduced, referred to as method of separation in the following, which provides accurate spectrum resolution in space at an optimum localization in frequency. Third, a joint strategy for non-separable fields is proposed, which is based on partitioning the space-frequency domain into several sub-spectra that have to be separable only within themselves and can thus be treated consecutively by the method of separation. Fourth, the presented methods are applied for the estimation of benchmark spectra with different bandwidths and frequency content, comprising a modulated Kanai–Tajimi spectrum [13,37] and a practical example of geometric imperfections in an I-section flange [11]. The results demonstrate weaknesses of the established techniques, i.e. the limitation of simultaneous space-frequency localization or the appearance of negative spectral density, and the advantages of the proposed method in terms of accurate space-frequency localization of its spectrum estimates, which is of particular importance in the presence of strong narrow-bandedness in frequency.

The present paper is organized as follows: Section 2 briefly summarizes relevant elements of stochastic process theory. Sections 3 and 4 contain a short overview of established space-frequency analysis techniques and an in-depth derivation of the method of separation, respectively. Section 5 illustrates difficulties of evolutionary spectrum estimation in the presence of strong narrow-bandedness and shows the results of each method for the imperfection example.

2. Some elements of stochastic process theory

A random field $h(x)$, equivalently known as a stochastic process in a time–frequency context, represents an ensemble of spatial functions, whose exact values are a priori indeterminate, but follow a predefined probability distribution [18,27,44]. It can be split into a deterministic mean $\mu(x) = E[h(x)]$ and a zero-mean random field $f(x) = h(x) - \mu(x)$. The stochastic structure of $f(x)$ is characterized by a number of higher moments, starting with the variance or mean square $E[|f(x)|^2]$, and an autocorrelation function $R(x,\tau)$, which determines for any $f(x)$ the dependence of neighbouring values as a function of their spatial distance τ [18,27,44]. The operator $E[\,]$ denotes mathematical expectation, which can be evaluated by simple ensemble averaging [18].

The Fourier transform $F(\omega)$, which decomposes a zero-mean random field $f(x)$ of length L by projecting it onto the basis of sines and cosines as a function of frequency ω [14,18,22], reads

$$F(\omega) = \frac{1}{2\pi} \cdot \int_0^L f(x) \cdot e^{-I\omega x} \, dx, \tag{2.1}$$

where I denotes the imaginary unit. The transformation of Eq. (2.1) can be evaluated in discrete form by the computationally efficient Fast Fourier Transform (FFT) [14,18]. In view of its trigonometric decomposition, $f(x)$ can be completely characterized by a two-sided power spectrum S [18,27,28,30,31,44], which is called homogeneous, if $S(\omega)$ depends only on frequency ω, and evolutionary, if $S(\omega,x)$ depends on both frequency ω and space x. Mathematically, the power spectrum is defined as the Fourier transform of the autocorrelation function $R(x,\tau)$ (Wiener–Khintchine theorem) [30,31]. An intuitive approach to the power spectrum is provided by its interpretation as the distribution of the mean square of the random field $f(x)$ over the space-frequency domain, so that it holds

$$E[|f(x)|^2] = 2 \int_0^\infty S(\omega, x) \, d\omega. \tag{2.2}$$

In this context, Eq. (2.2) is also denoted as the incremental energy or instantaneous power in space. Analogous to Eq. (2.2), the incremental energy in frequency is defined as

$$E[|F(\omega)|^2] = \int_0^L S(\omega, x) \, dx. \tag{2.3}$$

Eqs. (2.2) and (2.3) are also known as the marginal spectral densities of a random field [3]. The power spectrum is called narrowband, if the bulk of its energy is located only within a very small frequency band [18]. Additionally, the power spectrum satisfies spectral separability, if it can be multiplicatively decomposed into a homogeneous spectrum part $S(\omega)$ and a modulating spatial envelope $g(x)$ as

$$S(\omega, x) = S(\omega) \cdot g(x). \tag{2.4}$$

The corresponding random field is then called separable.

If the power spectrum $S(\omega,x)$ of a random field is known, an arbitrary number m of corresponding Gaussian random samples can be generated by the spectral representation method [9,35,36,39], which reads for a one-dimensional univariate zero-mean Gaussian random field

$$f^{(i)}(x) = \sqrt{2} \sum_{n=0}^{N-1} A_n \, \cos \, \left(\omega_n x + \phi_n^{(i)} \right), \tag{2.5}$$

with

$$A_n = \sqrt{2 \cdot S(\omega_n, x) \cdot \Delta\omega}, \tag{2.6a}$$
$$\omega_n = n \cdot \Delta\omega, \tag{2.6b}$$
$$\Delta\omega = \omega_{up}/N, \tag{2.6c}$$
$$A_0 = 0 \text{ or } S(\omega_0 = 0, x) = 0, \tag{2.6d}$$

where $i = 1,2,\ldots,m$ and $n = 0,1,2,\ldots,(N-1)$. The parameter ω_{up} is the cut-off frequency, beyond which the power spectrum is assumed to be zero, the integer N determines the discretization of the active frequency range, and $\phi_n^{(i)}$ denotes the $(i)^{th}$ realization of N independent phase angles uniformly distributed in the range $[0, 2\pi]$. For non-Gaussian random fields, the translation field theory can be used to generate random samples from a simple transformation of an underlying Gaussian field [10,40].

The performance of the evolutionary spectrum estimation methods to be presented in the following is tested by a uniformly modulated Kanai–Tajimi spectrum, which is defined according to Eq. (2.4) by its separable components

$$S(\omega) = \frac{1 + 4\varsigma^2 \left(\frac{\omega}{\omega_0}\right)^2}{\left[\left(1 - \left(\frac{\omega}{\omega_0}\right)^2\right)^2 + \left(2\varsigma \frac{\omega}{\omega_0}\right)^2 \right]}, \tag{2.7}$$

$$g(x) = \frac{e^{-0.25x} - e^{-0.5x}}{0.25}. \tag{2.8}$$

Parameters $\omega_0 = 10\,\text{rad/mm}$ and $\varsigma = 0.24$ represent the natural frequency and the damping ratio, respectively. The Kanai–Tajimi spectrum of Eq. (2.7) has been widely applied in a time–frequency context for the stochastic simulation of seismic ground acceleration, and various modulating terms leading to both separable and non-separable spectra can be found in the literature [13,16]. The specific values for ω_0 and ς in conjunction with the exponential modulating function of Eq. (2.8) are adopted from [37] and yield a power spectrum with equally pronounced evolution in space and frequency directions, therefore representing a suitable benchmark for evolutionary estimation techniques (see Figs. 1 and 2). In view of the energy interpretation of the spectrum, Eq. (2.7) can be conceived of as the incremental energy distribution in frequency direction, which does not change its shape, but is merely modulated in amplitude along the spatial axis by Eq. (2.8).

For a performance test in the non-separable case, a composed benchmark spectrum is defined as
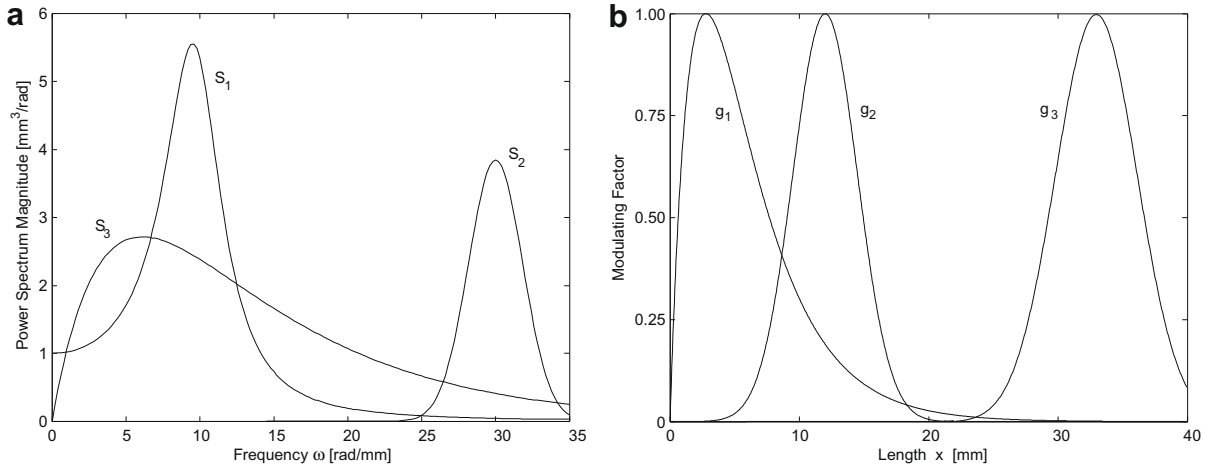
Fig. 1. Analytical components of the Kanai–Tajimi and composed benchmark spectra: (a) homogeneous spectra $S_i(\omega)$; and (b) modulating envelopes $g_i(x)$.
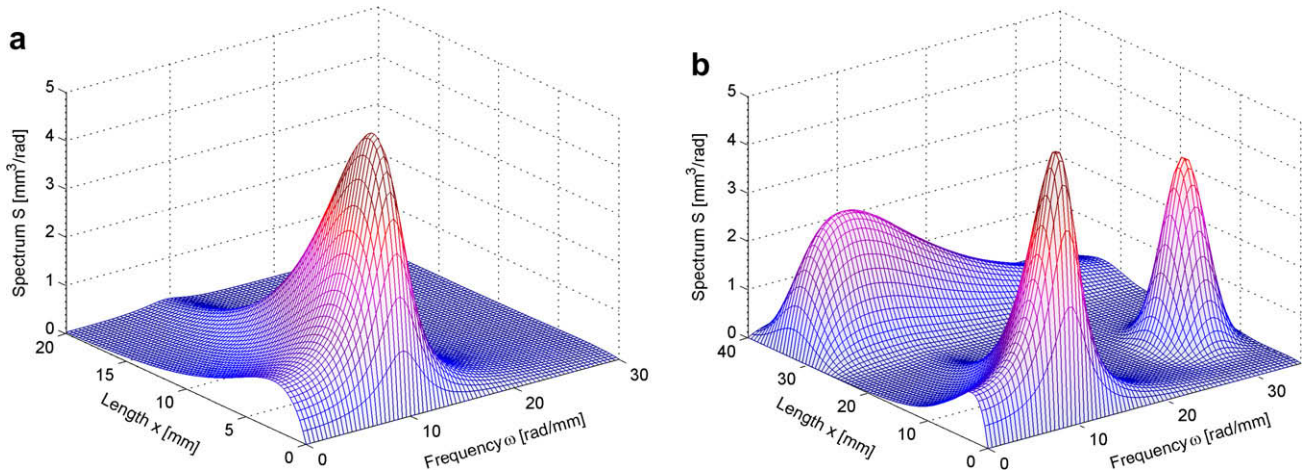

Fig. 2. Analytical reference solutions of the two benchmark spectra: (a) exact separable Kanai–Tajimi spectrum; and (b) exact non-separable composed spectrum.

$$S(\omega, x) = \sum_{i=1}^{3} S_i(\omega) \cdot g_i(x). \tag{2.9}$$

The first component of Eq. (2.9) is the modulated Kanai–Tajimi spectrum as defined by Eqs. (2.7) and (2.8); the second and third components are spectra of exponential type defined by pairs

$$S_2(\omega) = \frac{e^{-0.15(-\omega+24)^2}}{0.26} \quad \text{and} \quad g_2(x) = e^{-0.08(-x+12)^2}, \tag{2.10}$$

$$S_3(\omega) = \frac{e^{-0.1\omega} - e^{-0.25\omega}}{0.12} \quad \text{and} \quad g_3(x) = e^{-0.03(-x+30)^2}. \tag{2.11}$$

The first two pairs $[S_i, g_i]$ Eqs. (2.7), (2.8) and (2.10) again represent spectrum components with pronounced evolution in both space and frequency directions (see Figs. 1 and 2). The complete composed spectrum is non-separable, emphasized by the third pair Eqs. (2.11) with its longer ridge in frequency, but can be partitioned into sub-spectra that are separable within themselves, which makes it a suitable benchmark for the joint strategy.

The homogeneous parts $S_i(\omega)$ and the spatial envelopes $g_i(x)$ as well as the corresponding separable and non-separable benchmark spectra are illustrated in Figs. 1 and 2, respectively, and provide reference solutions in the following performance tests. Each benchmark spectrum is used in the spectral representation formula Eq. (2.5) to generate 10,000 corresponding random field samples $f^{(i)}(x)$, $i = 1, \ldots, 10{,}000$. Estimates of the analytical benchmark spectra are obtained by substituting $f^{(i)}(x)$ into the estimation methods introduced in the following, which can then be assessed by comparing the results with the initial exact spectra.

3. Existing methods for evolutionary power spectrum estimation

The homogeneous Fourier estimation of a power spectrum is a standard method [27,28,30,44], which can be obtained from a series of samples $f^{(i)}(x)$ by the so-called periodogram

$$\tilde{S}_h(\omega) = E\left[\frac{1}{2\pi L} \cdot \left| \int_0^L f^{(i)}(x) \cdot w\left(x - \frac{L}{2}\right) \cdot e^{-I\omega x} dx \right|^2 \right], \tag{3.1}$$

with L being the total sample length and window w centered at $x = L/2$. The homogeneous spectrum estimate $\tilde{S}_h(\omega)$ of the evolutionary Kanai–Tajimi benchmark obtained from 10,000 samples $f^{(i)}(x)$ is shown in Fig. 3. Whereas the energy distribution in frequency direction is predicted correctly, the spatial location of the energy peak is lost, since the Fourier transform in Eq. (3.1) averages the energy variation in space over the whole length L. To preserve this spatial information, samples $f^{(i)}(x)$ have to be transferred into evolutionary power spectra, for which different established methods of time–frequency analysis are available today [2,3] that are briefly reviewed in the following.
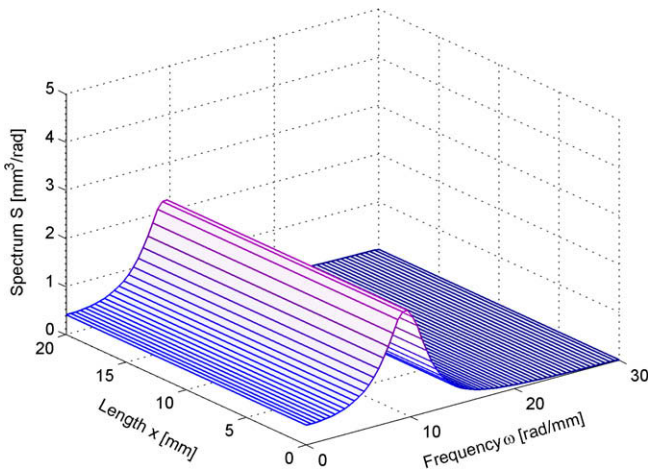
Fig. 3. Periodogram based estimate of the Kanai–Tajimi spectrum.

3.1. The short-time Fourier transform

The most common approach is based on the short-time Fourier transform (STFT), also referred to as the moving window or Gabor transform [2]. The basic idea of STFT is to emphasize the samples $f^{(i)}(x)$ at a distinct spatial position $x = \chi$, whose local properties are to be studied, and to suppress them at positions farther away from χ. This is achieved by multiplying the samples with a window $w(x - \chi)$ of finite width T centered at the position of interest χ. The window is then moved along the spatial axis, usually at n equally-spaced positions $x = \chi_j, j = 1 \ldots, n$, and the Fourier transform is applied at each χ_j. This strategy results in homogeneous spectrum components $\tilde{S}_j(\omega, x)$ for each χ_j

$$\tilde{S}_j(\omega, x) = E\left[\frac{1}{2\pi T} \cdot \left| \int_{\chi-T/2}^{\chi+T/2} f^{(i)}(x) \cdot w\left(x - \chi_j\right) \cdot e^{-I\omega x} dx \right|^2 \right]. \qquad (3.2)$$

The complete evolutionary spectrum estimate, also known as the spectrogram, can be obtained by combining all components $j = 1 \ldots, n$. The basic limitation of the method is its inability to achieve simultaneous localization in both frequency and space due to the uncertainty principle [2,3]. Originally motivated by Heisenberg's observations in quantum mechanics, the uncertainty principle has turned out to be a general property of Fourier analysis [29,41]. It states that the two components of a Fourier transform pair, such as a sample $f^{(i)}(x)$ and its squared windowed Fourier transform $\tilde{S}$ of Eq. (3.2), cannot be completely localized at the same time [2,3,18,29,41]. This means that if the spatial resolution is increased by shortening the window width T, the frequency localization of the spectrum deteriorates. In turn, if the width T is increased, frequencies are resolved better, but the spatial localization is reduced.

The results of the STFT based estimation for the two benchmark problems are shown in Fig. 4. Due to the uncertainty principle, a compromise in the spatial localization of the window function has to be chosen, that allows for a fair localization in space without distorting the frequency localization too severely. For the Kanai–Tajimi spectrum in Fig. 4a, a simple non-overlapping rectangular window [2,3,27]

$$w(x) = \begin{cases} 1 & -T/2 \leqslant x \leqslant T/2, \\ 0 & \text{elsewhere}, \end{cases} \qquad (3.3)$$

centered at 16 equally-spaced positions χ_j is applied. The effect of the uncertainty principle can be decreased by using special window functions [2,3,27], such as the Hamming window

$$w(x) = \begin{cases} 0.53836 - 0.46164 \; \cos\left(\frac{2\pi \; (x+T/2)}{T} \right) & -T/2 \; \leqslant \; x \; \leqslant \; T/2, \\ 0 & \text{elsewhere}. \end{cases} \qquad (3.4)$$

The application of a non-rectangular function Eq. (3.4) reduces the signal levels at the beginning and end of the window, leading to an energy bias called window-processing loss, which can be reduced by letting successive windows partly overlap into preceding ones [14,22]. This is illustrated in Fig. 4b by the STFT based estimate of the composed spectrum, for which six equally-spaced Hamming windows of width $T = L/3$ have been chosen, leading to an overlap of $L/12$ and a smoother spectrum surface.

3.2. The harmonic wavelet transform

A relatively new approach to space-frequency analysis is provided by the theory of wavelets [5,15]. For the joint space-frequency representation of evolutionary power spectra, harmonic wavelets developed by Newland [18–21] have proved to be especially suitable due to their exact box-like Fourier spectrum. The spatial window-like representation of the generalized harmonic wavelet functions can be summarized as

$$w_{m,n}\left(x - \frac{k}{n-m} \right) = \frac{e^{In2\pi\left(x - \frac{k}{n-m}\right)} - e^{Im2\pi\left(x - \frac{k}{n-m}\right)}}{I2\pi(n-m)\left(x - \frac{k}{n-m}\right)}, \qquad (3.5)$$
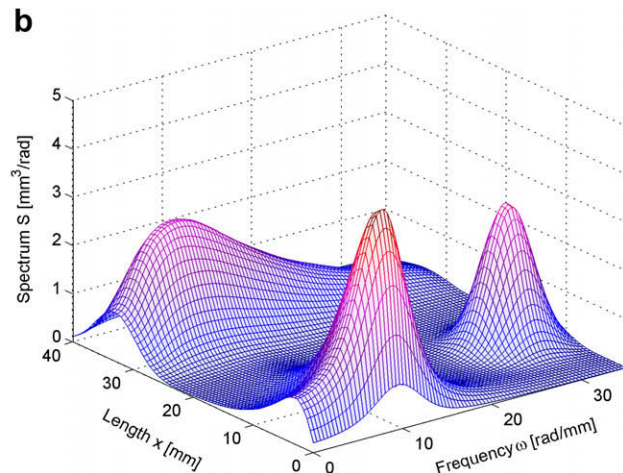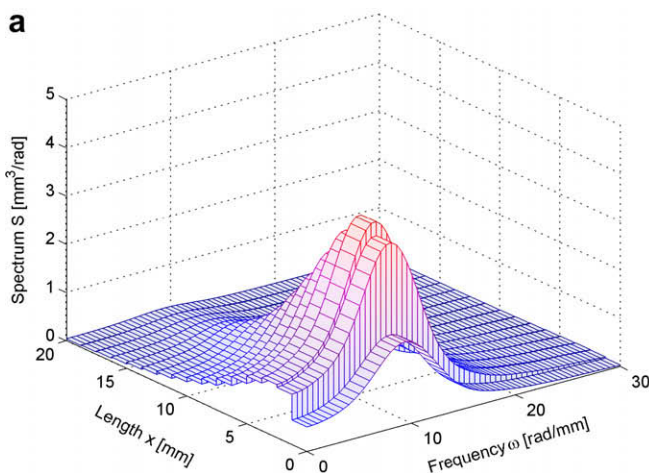

Fig. 4. STFT based power spectrum estimates of the two benchmark spectra: (a) separable Kanai–Tajimi spectrum; and (b) non-separable composed spectrum.

where the frequency scales (m,n) consist of touching, but not overlapping pairs of integers, controlling the frequency bandwidth of each wavelet function. The variation of k and (m,n) leads to a translation in space and dilation in frequency, respectively. Wavelets Eq. (3.5) can be interpreted as a collection of window functions that are mutually orthogonal, so that a generalized wavelet transform of a series of samples $f^{(i)}(x)$ can be constructed as

$$a^{(i)}_{(m,n),k} = (n-m) \int_0^L f^{(i)}(x) \, w_{m,n} * \left(x - \frac{k}{n-m}\right) \, dx, \qquad (3.6)$$

where (*) denotes complex conjugation. Because of the localized amplitudes of harmonic wavelets of the same frequency scale (m,n) at different positions $(x - k/(n-m))$, corresponding wavelet coefficients $a^{(i)}_{(m,n),k}$ can be used to distinguish local events of samples $f^{(i)}(x)$ at the same frequency. On this basis, Spanos and co-workers [37,43] have recently shown that an evolutionary power spectrum can be estimated from the wavelet coefficients Eq. (3.6) as

$$\tilde{S}_{(m,n),k} = \frac{4E\left[|a^{(i)}_{(m,n),k}|^2\right]}{n-m}. \qquad (3.7)$$

This formula defines the localized spectral density in the discrete space-frequency regions

$$\frac{m2\pi}{L} \leqslant \omega < \frac{n2\pi}{L} \text{ and } \frac{kL}{n-m} \leqslant x < \frac{(k+1)L}{n-m}, \qquad (3.8)$$

where $k = 0\ldots,(n-m-1)$ determines the coupling between space and frequency localization.

Analogous to Fourier analysis, the uncertainty principle limits simultaneous space-frequency localization in wavelet analysis [15], which is illustrated by the interdependence of space and frequency resolution in Eqs. (3.8). It allows either for a fine resolution in frequency, if differences in scales (m,n) are small, or for a fine resolution in space, if differences in scales (m,n) are large. The wavelet based estimate for the Kanai–Tajimi benchmark is shown in Fig. 5, showing reasonable localization due to a compromise in space-frequency resolution.

3.3. The Wigner–Ville transform

A qualitatively different approach is provided by the Wigner–Ville transform [2,3,17], which yields the following evolutionary spectrum expression from a series of samples $f^{(i)}(x)$

$$\tilde{S}(\omega,x) = E\left[\frac{1}{2\pi} \cdot \int_0^L f^{(i)}\left(x + \frac{\tau}{2}\right) \cdot f^{(i)}\left(x - \frac{\tau}{2}\right) \cdot e^{-l\omega\tau} \, d\tau\right], \qquad (3.9)$$

where τ is a shifting parameter. Eq. (3.9) can be interpreted as the Fourier transform of an autocorrelation estimate, defined as [18,27]

$$R(x,\tau) = E\left[f^{(i)}\left(x + \frac{\tau}{2}\right) \cdot f^{(i)}\left(x - \frac{\tau}{2}\right)\right], \qquad (3.10)$$

and thus provides a power spectrum estimation on the basis of the Wiener–Khintchine theorem [30,31].

The major strength of the method is the accurate representation of the marginal densities of Eqs. (2.2) and (2.3), which is a key indicator for accurate space-frequency localization. Drawbacks are the large number of localized oscillations [2] and the potential ability of the Wigner–Ville method to yield negative spectral values, which contradicts the mathematical definition of the power spectrum and its physical energy interpretation [2,3]. The Wigner–Ville estimate of the Kanai–Tajimi benchmark is shown in Fig. 6. Due to the large number of 10,000 input samples, localized oscillations responsible for the irregular surface, and negative spectrum values are considerably reduced, leading to good accuracy with respect to the analytical reference Fig. 2a.
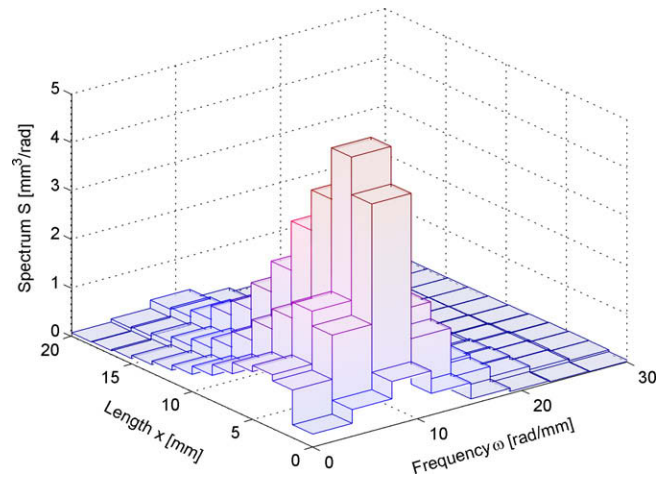

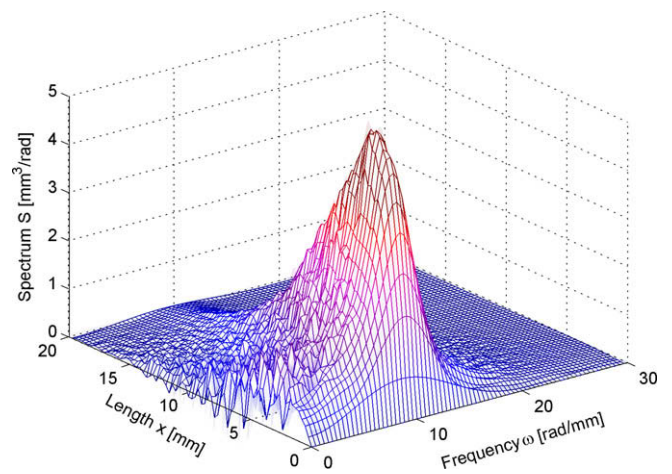**Fig. 5.** Harmonic wavelet based estimate of the Kanai–Tajimi spectrum.

Fig. 6. Wigner–Ville based estimate of the Kanai–Tajimi spectrum.

4. The method of separation: robust evolutionary spectrum estimation of separable random fields

Besides existing space-frequency analysis techniques, a further method is introduced in the following. It is generally valid for the estimation of separable power spectra, but in particular designed to cope with the challenge of simultaneous localization in space and frequency, which is of major importance for the accurate evolutionary spectrum estimation of strongly narrow-band random fields.

4.1. Theory and derivation

The present approach, which will be called method of separation in the following, assumes that input samples $f^{(i)}(x)$ represent a separable or at least approximately separable random field. The essential advantage of this assumption in the present case is the breakdown of the combined evolutionary spectrum estimation into a frequency and a spatial part, which can be dealt with separately. The definition of spectral separability Eq. (2.4) allows that its multiplicative components can be chosen arbitrarily from a group of pairs $[\acute{S};\acute{g}]$ that satisfy with respect to the original components $[S;g]$

$$S'(\omega) = \lambda \cdot S(\omega), \tag{4.1a}$$

$$g'(x) = \frac{1}{\lambda} \cdot g(x), \tag{4.1b}$$

where λ is an arbitrary positive number. Eq. (4.1) constitute sets of geometrically similar functions, whose energy content, i.e. area under the curves, is varied by λ, but whose energy distributions over frequency or space, i.e. the relative shapes of the curves, remain the same. The product of Eq. (4.1) yields always the correct evolutionary spectrum $S(\omega,x)$ of Eq. (2.4). In the method of separation, the spectrum component Eq. (4.1a) is chosen as the homogeneous Fourier power spectrum

$$S_h(\omega) = \frac{1}{L} \cdot \int_0^L S(\omega, x)\, dx = \lambda_h \cdot S(\omega), \tag{4.2}$$

corresponding to the frequency content of the evolutionary spectrum $S(\omega,x)$ averaged over the signal length L. Its counterpart $g_h(x)$ can be obtained from Eq. (4.1b) by factor

$$\lambda_h = \frac{1}{L} \cdot \int_0^L g(x)\, dx. \tag{4.3}$$

The evolutionary spectrum $S(\omega,x)$ in the method of separation is thus decomposed into

$$S(\omega, x) = S_h(\omega) \cdot g_h(x). \tag{4.4}$$

An estimate $\tilde{S}_h(\omega)$ of the homogeneous Fourier power spectrum in Eq. (4.4) can be readily obtained from Eq. (3.1), where the frequency content of the separable input samples are averaged over their length L by the Fourier transform [3,18,27], which corresponds to the definition of $S_h(\omega)$ in Eq. (4.2). Accordingly, an estimate $\tilde{g}_h(x)$ for the spatial envelope can be derived from the mean square of samples $f^{(i)}(x)$. The basic analytical expression is found from Eq. (2.2) as

$$E\left[|f(x)|^2\right] = 2\int_0^\infty S_h(\omega)\, g_h(x)\, d\omega = g_h(x) \cdot 2 \int_0^\infty S_h(\omega)\, d\omega. \tag{4.5}$$

The estimate $\tilde{g}_h(x)$ can then be obtained by replacing in Eq. (4.5) the analytical homogeneous spectrum $S_h(\omega)$ and mean square $E[|f(x)|^2]$ by the corresponding estimates, which yields

$$\tilde{g}_h(x) = \frac{E\left[|f^{(i)}(x)|^2\right]}{2\int_0^\infty \tilde{S}_h(\omega)\, d\omega}. \tag{4.6}$$

The final estimate of the spectrum can now be established by replacing the analytical expressions in Eq. (4.4) by their estimates $\tilde{S}_h(\omega)$ of Eq. (3.1) and $\tilde{g}_h(x)$ of Eq. (4.6), which yields

$$\tilde{S}(\omega, x) = E\left[|f^{(i)}(x)|^2\right] \cdot \frac{\tilde{S}_h(\omega)}{2\int_0^\infty \tilde{S}_h(\omega)\, d\omega}. \tag{4.7}$$

Factor $1/2$ in the right-hand side fraction is necessary, because Eq. (4.7) takes into account only one side of the symmetric two-sided power spectrum. The validity of Eq. (4.7) can be succinctly illustrated by energy considerations. The right-hand side fraction contains the estimate $\tilde{S}_h(\omega)$ in the numerator, which is normalized by the denominator in the sense that its total energy content, i.e. the area under the curve $\tilde{S}_h(\omega)$, is a constant of 1. This can be trivially verified by integration of the right-hand side fraction in Eq. (4.7) over frequency as

$$\int_0^\infty \frac{\tilde{S}_h(\omega)}{\int_0^\infty \tilde{S}_h(\omega) d\omega}\, d\omega = 1. \tag{4.8}$$

The left-hand side contains the mean square of samples $f^{(i)}(x)$, which due to Eq. (2.2) is an estimate of the incremental energy in space. Hence, Eq. (4.7) can be interpreted at each position x as the distribution of the mean square over the frequency domain

by a normalized homogeneous spectrum. This makes the method of separation a direct implementation of the initial intuitive concept of the power spectrum.

4.2. A joint strategy for non-separability

A limitation of the method of separation in view of its application to general power spectra is its separability assumption. Complex benchmark spectra such as chirps [2,3] cannot be estimated properly, since Eq. (4.7) forces their changing energy distribution in frequency direction into a separable unified form. The capacity of the present method can be considerably increased by a joint strategy based on the partitioning of the space-frequency domain into several parts, which have to be separable only within themselves. Thus, the hypothesis of spectral separability can be replaced by a much weaker assumption, which requires the non-separable spectrum to be decomposable or approximately decomposable in several separable sub-spectra only. The space-frequency localization of each sub-spectrum can then be refined by applying the method of separation across corresponding sub-regions. The reassembly of all sub-spectra provides the final spectrum estimate for the complete space-frequency domain.

Rectangular and non-overlapping sub-regions can be defined by corresponding pairs of space and frequency segments $[x_r,x_{r+1}]$ and $[\omega_s,\omega_{s+1}]$, respectively (see Fig. 7). On the one hand, this can lead to p separable sub-spectra that are aligned along the spatial axis in successive segments $[x_r,x_{r+1}]$, $r = 1, \ldots, p$. The simple separation of the series of input samples $f^{(i)}(x)$ according to the spatial segments $[x_r,x_{r+1}]$ allows for a direct application of the method of separation in the p sub-regions. On the other hand, this can lead to q separable sub-spectra aligned along the frequency axis in successive segments $[\omega_s,\omega_{s+1}]$, $s = 1, \ldots, q$. In the case of q-partitioning, the method of separation has to be modified, since the estimation of q spatial envelopes $\tilde{g}_h(x)^s$, $s = 1, \ldots, q$ by Eq. (4.6) requires a decomposition of samples $f^{(i)}(x)$ according to their contribution to the respective frequency segment $[\omega_s,\omega_{s+1}]$ in the form

$$\tilde{g}_h(x)^s = \frac{E\left[|\varphi\left[f^{(i)}(x)\right]_{\omega_s}^{\omega_{s+1}}|^2\right]}{2\int_{\omega_s}^{\omega_{s+1}} \tilde{S}(\omega)\, d\omega}, \tag{4.9}$$

$\varphi[]_{\omega_s}^{\omega_{s+1}}$ denotes a filter operator, separating the trigonometric components within frequency bandwidth $[\omega_s,\omega_{s+1}]$ from the complete input samples $f^{(i)}(x)$. With Eq. (2.2), the numerator of Eq. (4.9) can be expressed as the integration of the evolutionary spectrum $S(\omega,x)$ over the respective frequency segment $[\omega_s,\omega_{s+1}]$ of the sub-
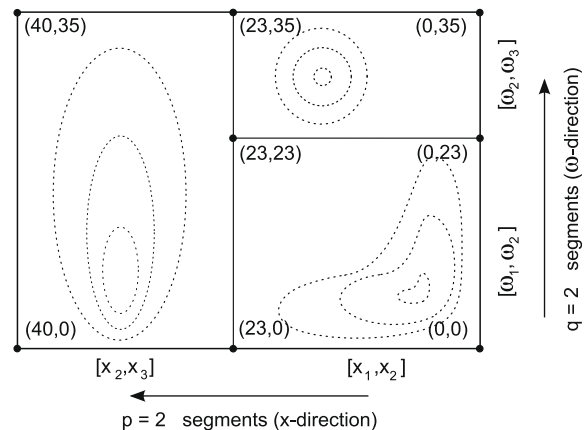

Fig. 7. *p*- and *q*-partitioning of the space-frequency domain for the composed spectrum.

region. $S(\omega,x)$ can then be replaced in each sub-region by its harmonic wavelet based estimate $\tilde{S}_{(m,n),k}$ Eq. (3.7). This leads to

$$\tilde{g}_h(x)^s = \frac{\int_{\omega_s}^{\omega_{s+1}} S(\omega,x)\,d\omega}{2\int_{\omega_s}^{\omega_{s+1}} \tilde{S}(\omega)\,d\omega} = \frac{2\int_{\omega_s}^{\omega_{s+1}} E\left[|a^{(i)}_{(m,n),k}|^2\right] d\omega}{(n-m)\int_{\omega_s}^{\omega_{s+1}} \tilde{S}(\omega)\,d\omega},$$
(4.10)

where $a^{(i)}_{(m,n),k}$ are the wavelet coefficients of each input sample $f^{(i)}(x)$ according to Eq. (3.6). The key point of Eq. (4.10) is the appropriate choice of the scales (m,n), so that the partitioning of the wavelet frequency bandwidths coincide with segments $[\omega_s, \omega_{s+1}]$, as

$$m = \frac{\omega_s}{2\pi} \text{ and } n = \frac{\omega_{s+1}}{2\pi}.$$
(4.11)

Eqs. (4.11) ensure the accurate filtering of the input samples $f^{(i)}(x)$, since corresponding wavelet coefficients $a^{(i)}_{(m,n),k}$ perform a separation of the energy contained in the frequency bands $[\omega_s, \omega_{s+1}]$.

A fundamental prerequisite of the proposed methodology is the apriori knowledge of the spectrum shape, so that separable sub-spectra can be detected and an adequate partitioning of the space-frequency domain can be chosen. In a general application with samples from an unknown non-separable power spectrum, the decision how to sub-divide the space–frequency domain best can be based on preliminary spectrum estimation across the com-

plete domain by one of the existing spectrum estimation techniques introduced in Section 3.

4.3. Performance test with benchmark spectra and comparison with established techniques

The general validity of the method of separation is first tested by the Kanai–Tajimi benchmark. The complete spectrum estimate of the method of separation along with the two principal components of Eq. (4.7), i.e. the estimated mean square and the estimated normalized frequency distribution, are shown in Figs. 8a and 9, respectively. The method of separation captures exact spectrum gradients and peak values (Fig. 2a) considerably better than STFT and wavelet transforms (Figs. 4a and 5) and leads to a more regular spectrum surface than the Wigner–Ville transform (Fig. 6). The geometric similarity of the component estimates in Fig. 9 with respect to the analytical components in Fig. 1 illustrates the validity of the fundamental expressions in Eq. (4.1). The marginal densities of Eqs. (2.2) and (2.3), which are an excellent indicator for the quality of space and frequency localization, respectively [3], are plotted in Fig. 10. The method of separation and the Wigner–Ville transform are able to reproduce the analytical incremental energies exactly due to their accurate localization properties in both space and frequency directions, whereas STFT and harmonic wavelet based
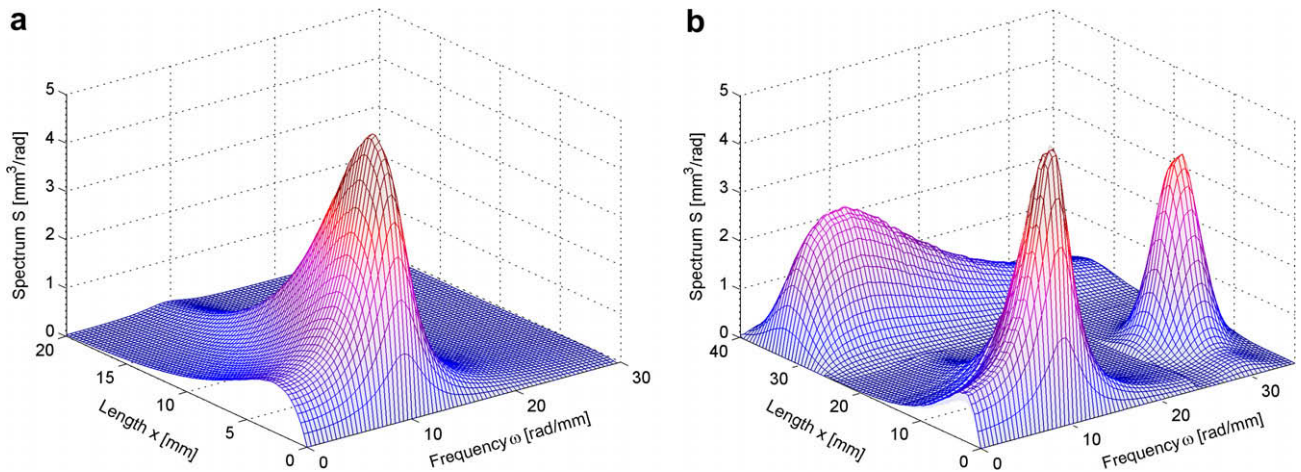

Fig. 8. Method of separation based power spectrum estimates of the two benchmark spectra: (a) separable Kanai–Tajimi spectrum; and (b) non-separable composed spectrum.
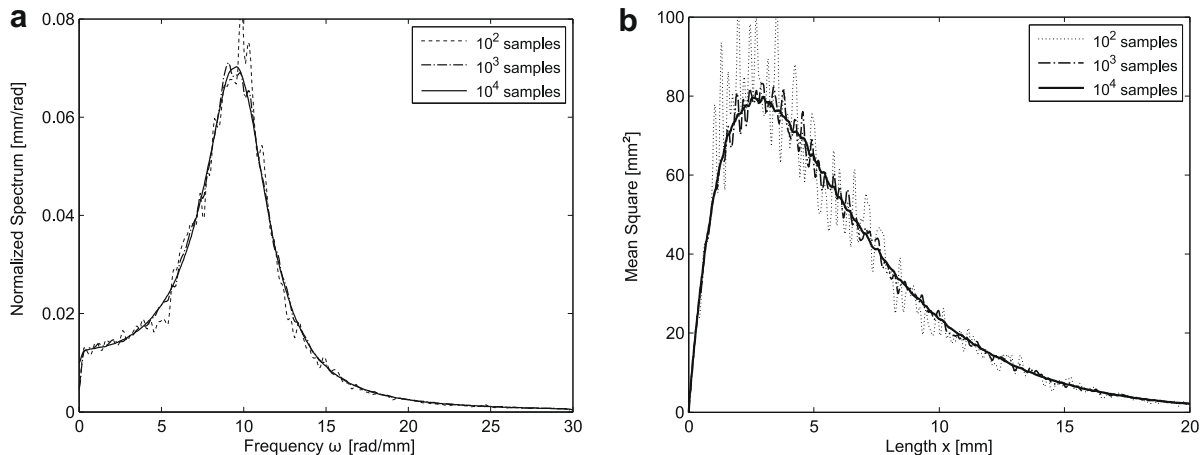

Fig. 9. Frequency and spatial components of the method of separation for the Kanai–Tajimi spectrum from different sample sizes: (a) estimates of frequency distribution (right-hand side fraction of Eq. (4.7)); and (b) estimates of mean square (left-hand side of Eq. (4.7)).
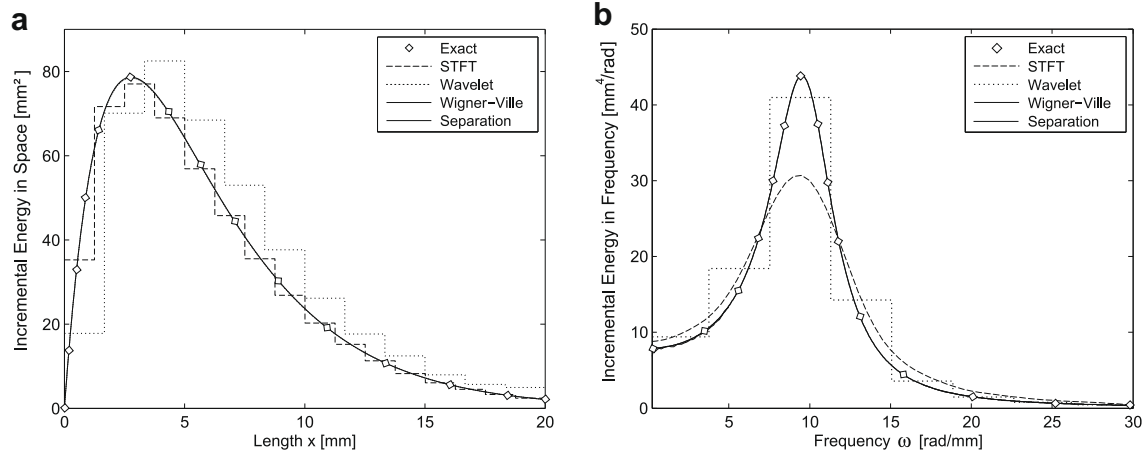
Fig. 10. Marginal densities (incremental energies) for the Kanai–Tajimi estimates: (a) marginal density in space (mean square); and (b) marginal density in frequency.
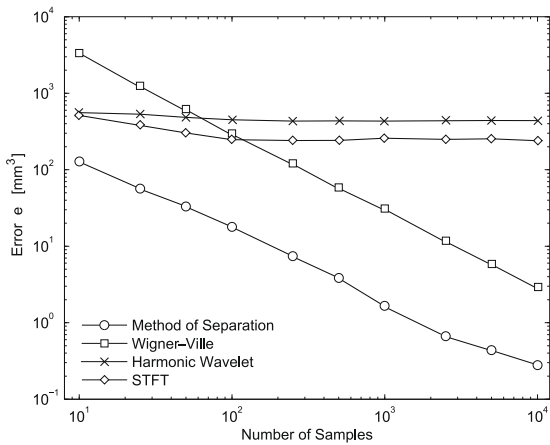

Fig. 11. Convergence of the examined estimation techniques for the Kanai–Tajimi spectrum.

methods exhibit observable deviations from the exact solutions as a consequence of the uncertainty principle. The marginal densities in space and frequency for STFT and wavelet methods reflect the quality of the trade-off between spatial and frequency localization. Stochastic convergence in a Monte-Carlo sense [27] is tested by the

squared difference between exact analytical and estimated Kanai–Tajimi spectra S_{ex} and $\tilde{S}_m$, respectively, integrated over the space-frequency domain in the form

$$e(m) = \int_0^\infty \int_0^L \left(S_{ex} - \tilde{S}_m \right)^2 dx d\omega. \tag{4.12}$$

The error e Eq. (4.12), which depends on the number m of input samples $f^{(i)}(x)$, $i = 1, \ldots, m$ used for the computation of $\tilde{S}_m$, is plotted in Fig. 11 for each estimation method. Whereas STFT and wavelet estimates do not converge due to the systematic error of the uncertainty principle, the method of separation achieves monotonic convergence, approaching the exact solution faster than the Wigner–Ville method. Thus, the method of separation based estimate of the Kanai–Tajimi spectrum is shown to be more accurate in terms of regularity of the spectrum surface, space-frequency localization and convergence towards the exact spectrum than the results of the established estimation techniques.

For the estimation of the non-separable composed spectrum, it is assumed here that the spectrum shape analytically defined by Eqs. (2.7) through (2.11) is unknown and the only information available consists of 10,000 samples of the corresponding random field generated by spectral representation. Thus, an apriori idea of the spectrum shape has to be obtained first for the adequate partitioning of the space-frequency domain, for example by application of the STFT approach. Based on its result in Fig. 4b, the three sep-
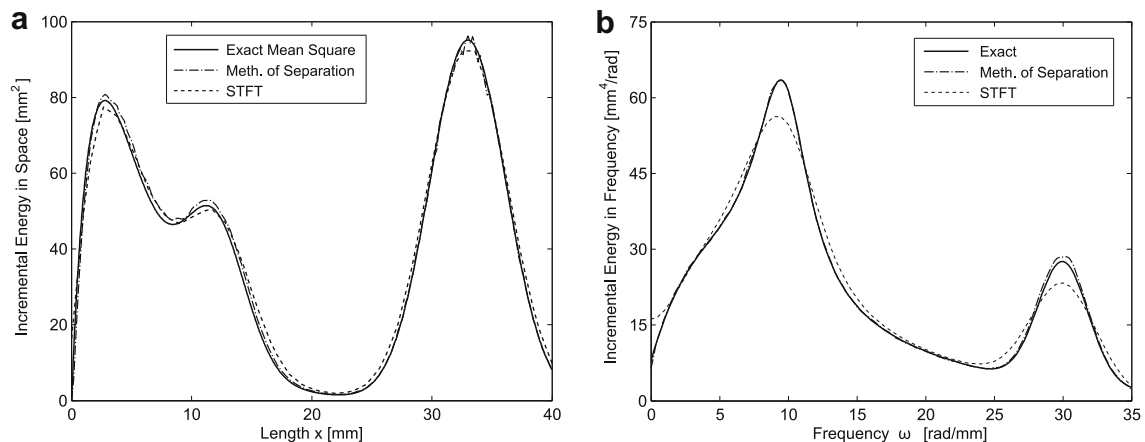

Fig. 12. Marginal densities (incremental energies) for estimates of the composed spectrum: (a) marginal density in space (mean square); and (b) marginal density in frequency.

arable sub-spectra can be clearly identified and the partitioning of the space-frequency domain can be chosen according to Fig. 7. The spectrum estimate resulting from the joint strategy for non-separability is shown in Fig. 8b. It captures the spectrum peaks in terms of maximum values and gradients better than the STFT based estimate of Fig. 4b, but exhibits slight discontinuities at the sub-region boundaries. The corresponding marginal densities in Fig. 12 demonstrate that the space-frequency localization achieved by the joint strategy and the method of separation is considerably improved in comparison to the STFT marginals. The slight deviation of the method of separation based results from the exact analytical solutions of Figs. 2b and 12 is due to the overlapping of some energy from neighbouring sub-regions, which introduces a slight non-separability of the benchmark spectrum within each sub-region.

5. Stochastic imperfection modeling in structures: accurate estimation of strongly narrow-band power spectra

The introduced space-frequency analysis techniques are now applied for the stochastic simulation of structural imperfections, where input samples typically are strongly narrow-band in frequency. The example problem considered here consists of six mea-

Fig. 13. The I-section beam experimentally investigated by Hasham and Rasmussen [11]: (a) perfect geometry of the I-section beam; (b) true geometry with 150× enlarged imperfections; and (c) measured flange edge imperfections δ.

surements of geometric imperfections in an I-section flange, from which an evolutionary power spectrum should be estimated. The measurements were obtained by surveying the flange edges of six nominally identical I-section beams of length $L = 2000$ mm [11]. They represent the deviation δ of the true flange edge position from perfect plate geometry along the beam axis as illustrated in Fig. 13. The zero-mean parts of the imperfection measurements represent six input samples $f^{(i)}(x), i = 1, \ldots, 6$, plotted in Fig. 14a. In the following, the validity of the hypothesis of spectral separability for the present example is first examined. Then, the aspects of spectral leakage, spectral dispersion and small sample size are discussed in detail. Finally, the performance of the presented techniques in the presence of strong narrow-bandedness are compared and assessed.

5.1. Spectral separability

The assumption of spectral separability in the method of separation introduces an error in case of non-separable input samples. Non-separability implies that the energy distribution over the frequency domain, i.e. the spectrum shape in frequency direction, differs along x, as illustrated by the non-separable composed spectrum Fig. 2b. In the case of the strongly narrow-band imperfection measurements, possible variations of energy distribution in frequency are considerably limited, since the main lobe is located only within a very small fixed bandwidth. This is illustrated by a STFT based spectrum estimate according to Eq. (3.2), obtained at six equally-spaced positions χ_j by a non-overlapping Hamming window of length $L/6$. The six individual STFT components plotted in Fig. 15 are normalized analogous to Eq. (4.8), so that they would coincide in case of exact spectral separability. The discrepancy between the plotted curves with respect to shape and amplitude thus indicates the degree of non-separability. Within the narrow-band main lobe, which ranges from 0 to around 0.03 rad/mm (see Fig. 15) and contains about 95% of the total energy, approximate spectral separability can be readily verified, since the six curves exhibit the same qualitative shape and diverge only slightly. Beyond the narrow-band main lobe, the curves show larger divergence, and hence indicate non-separability (see logarithmic plots in Fig. 15). Since the divergent parts of spectrum components cover only about 5% of the total energy, the present imperfection example can still be assumed to be approximately separable.

5.2. Spectral leakage and spectral dispersion

Fourier analysis of finite length signals is biased by two phenomena known as spectral leakage and spectral dispersion, which both lead to an unphysical frequency distribution of part of the signal's energy.

Spectral leakage results from the discrete nature of the finite length Fourier transform [14]. The FFT algorithm is constrained to operate on a finite set of N input values, sampled at the sampling rate $f_S = N/L$, and yields discrete frequency information at the following frequency points ω_j [14]

$$\omega_j = 2\pi \cdot \frac{j \cdot f_S}{N} = j \cdot \frac{2\pi}{L} \quad \text{with } j = 0, 1, 2, \ldots, N - 1. \quad (5.1)$$

In the present example, the measured imperfection signals consist of $N = 80$ points at a distance of 25 mm. Finite length Fourier transforms can correctly attribute only those energy components of the input signals, which precisely occur at the frequencies given in Eq. (5.1). Energy components of intermediate frequencies, however, tend to leak out away from their correct frequency positions. The discrete Fourier transform of strongly narrow-band functions is especially sensitive to leakage errors, since almost all of their frequency content is located between only a few discrete frequency
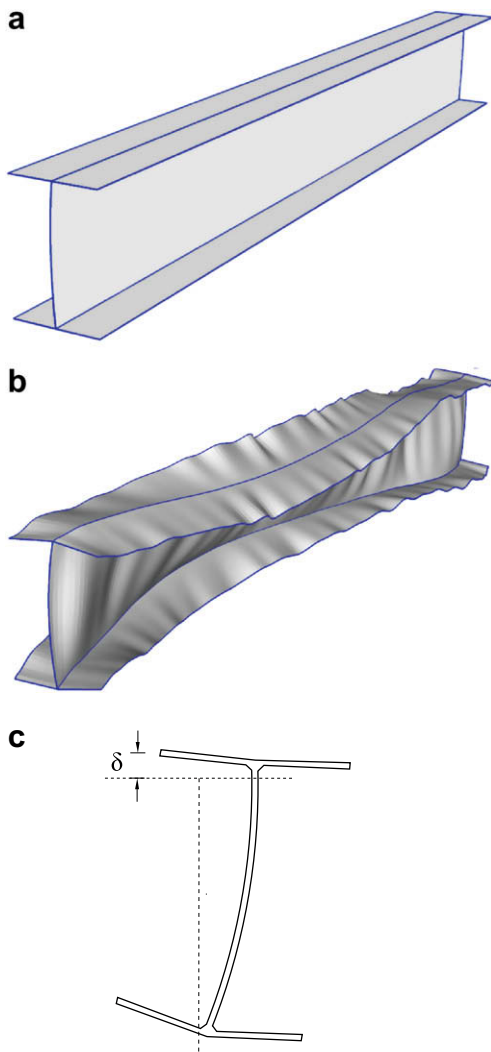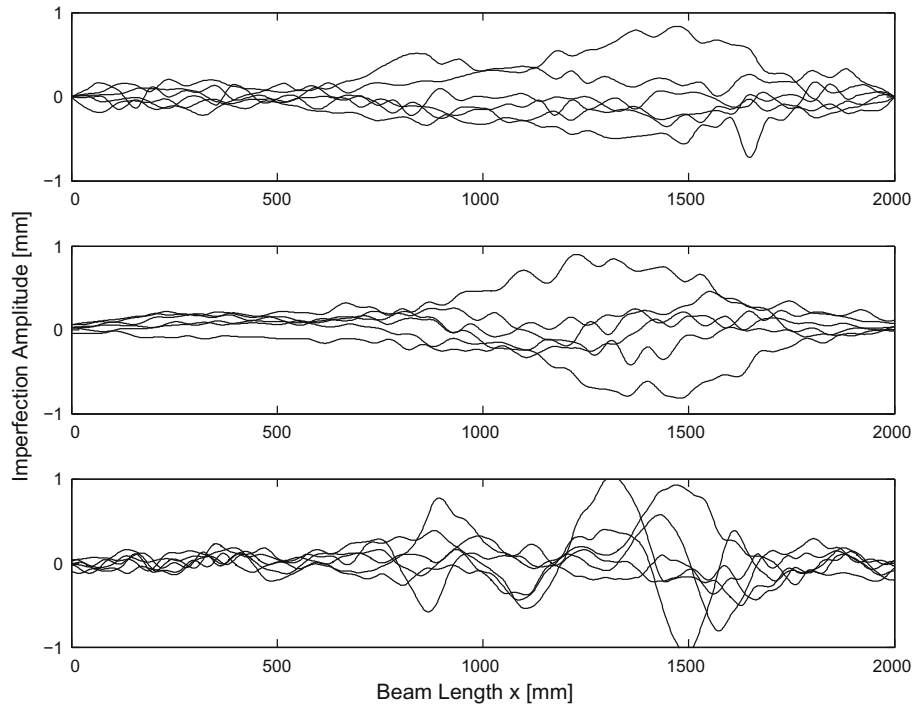
Fig. 14. Zero-mean parts of the input measurements $f^{(i)}(x)$ and six samples generated from method of separation and STFT based spectrum estimates: (a) zero-mean part of measurements; (b) method of separation based simulation; and (c) STFT based simulation.
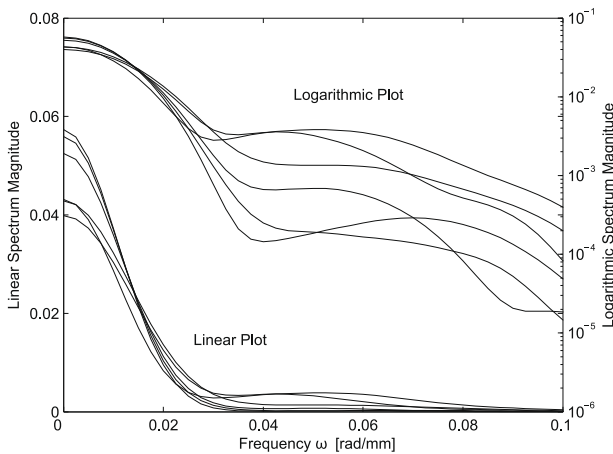

Fig. 15. STFT based spectrum components normalized by their incremental energy in space.
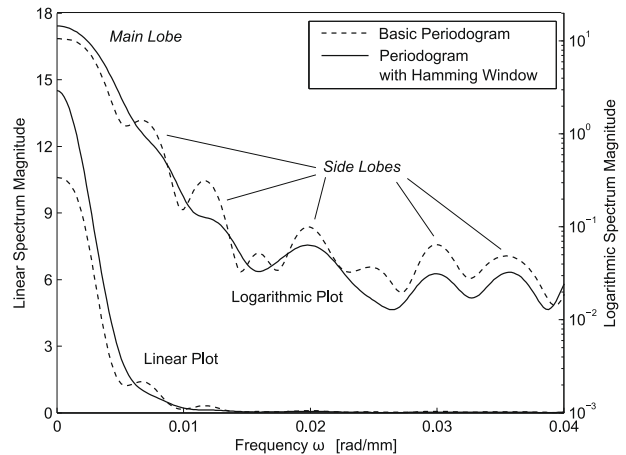

Fig. 16. Leakage from main lobe into side lobes in the periodogram.

points ω_j. The leakage sensitivity of the present example is illustrated in Fig. 16 by its periodogram Eq. (3.1). It consists of a main lobe between 0 and 0.005 rad/mm, which contains the correctly attributed energy, and unphysical periodic peaks at higher frequencies, known as side lobes, which contain the leaked energy. Windowing the input signals with the Hamming window Eq. (3.4) reduces the leakage effect [14] (see Fig. 16).

Spectral dispersion is a direct consequence of the uncertainty principle [2,3,29,41]. It occurs, when the signal length L is limited by the introduction of a finite length window to achieve better space-frequency resolution, such as in Eqs. (3.2) or (3.6). Its characteristic mechanism is succinctly illustrated in Fig. 17 for the present imperfection example. Localization in space of the mean square $E[|f^{(i)}(x)|^2]$ is obtained by applying a Hamming window centered at $\chi = L/2$, as shown in Fig. 17a. Comparison with Fig. 17b reveals that

an increase in spatial mean square localization, i.e. a decrease in window width T, necessitates spectral dispersion about $\omega = 0$ in the corresponding two-sided spectrum estimate $\tilde{S}(\omega)$ of Eq. (3.1). Strongly narrow-band spectra with evolutionary power in space are especially sensitive to this phenomenon, since their true bandwidths are considerably smaller than the frequency spread introduced by a window width, which has to be small enough for a reasonable localization in space.

5.3. Number of samples and spectral smoothing

In most practical applications, only a very limited number of measurements are available. The resulting insufficient ensemble averaging in the evaluation of the operator $E[]$ in Eq. (4.7) leads to spurious oscillations in the evolutionary spectrum estimate, due to localized under-and overestimation of the true spectrum
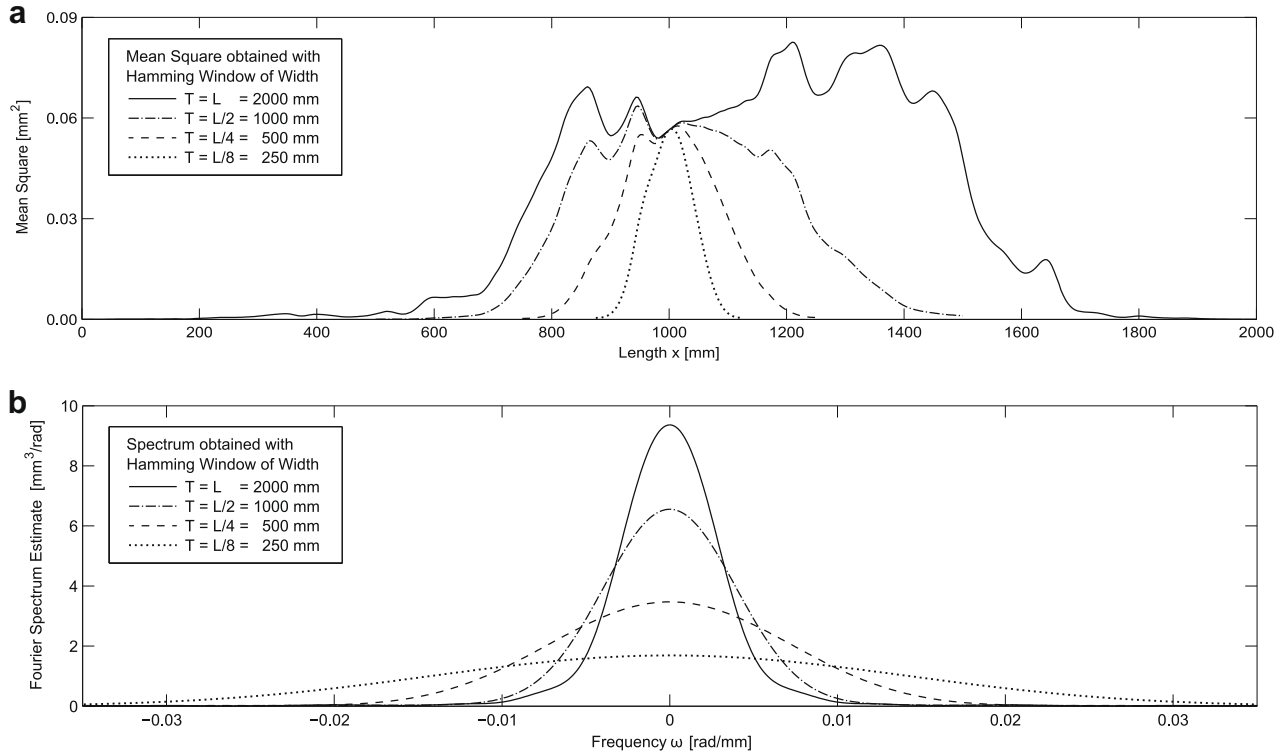
Fig. 17. Spectral dispersion in the imperfection example: (a) increase in localization in the mean square $E[-f^{(i)}(x)-^2]$ about $x = L/2$; and (b) decrease in localization in the two-sided spectrum estimate $\hat{S}(\omega)$ about $\omega = 0$.

(see Fig. 9). The spurious oscillations are stronger in spatial direction x, because the evaluation of the right-hand fraction implies an additional averaging of frequency content over length L (see Eq. (3.1)). An effective damping of the spurious oscillations in spatial direction can be accomplished by spectral smoothing algorithms, as for example proposed in [18] in the form

$$\hat{S}(\omega, x_k) = \frac{1}{2n+1} \sum_{m=-n}^{n} \tilde{S}(\omega, x_{k+m}), \tag{5.2}$$

where x_k denote sample points in space of the discrete spectrum representation and $\hat{S}$ is the smoothed spectrum. Eq. (5.2) can be imagined as a window, which is moved in small steps along the spatial axis, successively replacing the central spectrum values by the arithmetic average of all visible values. The empirical window size $(2n + 1)$ has to be chosen small enough not to distort the evolutionary trend, but large enough to effectively smoothen the spurious local oscillations.

5.4. Performance of available estimation techniques

The spectrum estimates of the corresponding imperfection example obtained from the wavelet, Wigner–Ville, and STFT based techniques and the method of separation are shown in Fig. 18. Motivated by the discussion of spectral leakage in Section 5.2, all measurements have been multiplied by a Hamming window prior to the application of Fourier transforms in order to prevent the development of side lobes. Note that the method of separation is not affected by a possible window-processing loss [14,22], because this effect cancels out in the right-hand side fraction of Eq. (4.7). The harmonic wavelet based estimate in Fig. 18a exhibits satisfactory localization in frequency direction, which can be obtained by the smallest possible difference in scales $n - m = 1$, but no localization in space due to the restriction of Eq. (3.8). The Wigner–Ville estimate in Fig. 18b can be expected to give an accurately localized

impression of the true power spectrum, but negative spectral density appears over large parts of the space-frequency domain. The estimates in Fig. 18a and b are thus inaccurate or unsuitable to be used in the framework of spectral representation. The STFT based estimate in Fig. 18c, which has been obtained with 16 overlapping Hamming windows of width $L/8$, exhibits good localization in space. However, in comparison to the Wigner–Ville and method of separation based estimates, which rely on a Fourier transform with full window width $T = L$, the STFT based estimate is severely biased in frequency direction by spectral dispersion. Its detrimental impact as discussed in Section 5.2 is succinctly summarized by corresponding marginal densities in Fig. 19, which illustrate an accurate reproduction of the evolutionary trend in space, but a severe spread of the main lobe in frequency.

The applicability of the method of separation requires at least approximate spectral separability of the input samples, which can be presumed for the present imperfection example as discussed in Section 5.1. The accurately localized estimation result of the method of separation is shown in Fig. 18d. Due to the small number of only 6 available measurements, spectral smoothing as discussed in Section 5.3 is applied, which results in the final smoothed estimate Fig. 18e. In view of spectral dispersion, the frequency localization in the Fourier transform of a strongly narrow-band function corresponds to the availability of a sufficiently long signal length L. Since the method of separation Eq. (4.7) allows the use of the full available length L in the Fourier transforms involved, its spectrum estimate thus guarantees an optimum frequency localization and a minimum spread of the energy distribution. The excellent space-frequency localization of the method of separation is further evidenced by its marginal densities in Fig. 19. The qualitative accordance of its energy distribution and peak values with the Wigner–Ville estimate Fig. 18b additionally supports the plausibility of the smoothed estimate Fig. 18e.

Finally, the STFT based spectrum estimate of Fig. 18c and the smoothed spectrum estimate of the method of separation of
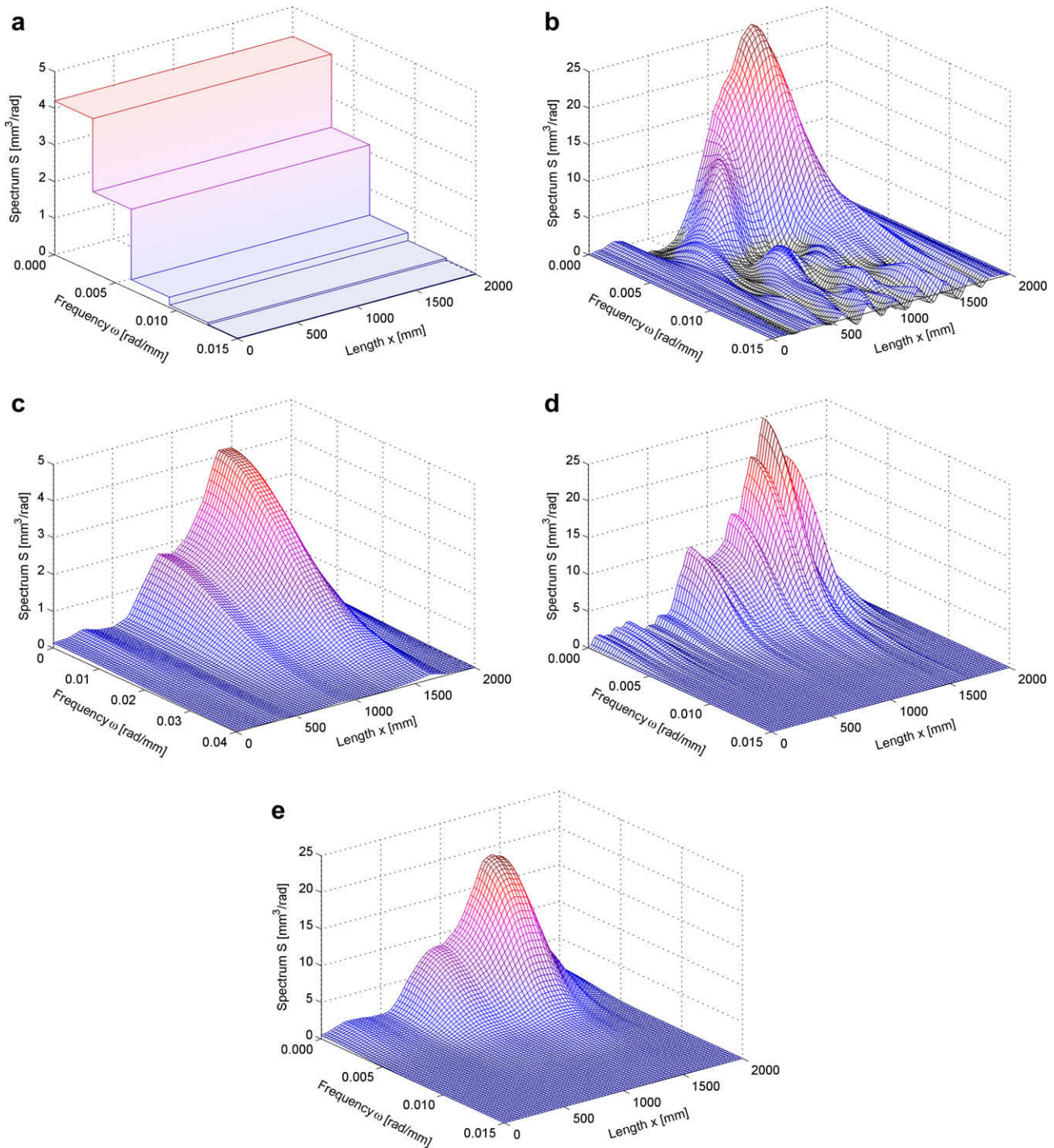
Fig. 18. Evolutionary spectrum estimates for the narrow-band imperfection example: (a) harmonic wavelet based estimate; (b) Wigner–Ville based estimate; (c) STFT based estimate; (d) method of separation based estimate; and (e) smoothed method of separation based estimate.

Fig. 18e are used to generate six random imperfection samples by spectral representation with Eq. (2.5), which are plotted in Fig. 14b for the method of separation and Fig. 14c for the STFT. The characteristic variation of measured imperfection amplitudes can be reproduced accurately by both groups of simulated samples. As a result of the large frequency spread in the STFT based spectrum, the wave-lengths in the corresponding samples in Fig. 14c largely deviate from the measurements in Fig. 14a, best illustrated by the frequent crossing of the zero line. The wave-lengths of the method of separation based samples in Fig. 14b can be observed to slightly underestimate the experimental wave-lengths in the interval

$x = [0, 500]$, which is likely to be a consequence of the spectral separability assumption discussed in Section 5.1. In general, they nonetheless correlate considerably better with the measured counterparts than the STFT based samples.

6. Summary and conclusions

The present paper is focused on space-frequency analysis techniques for the estimation of evolutionary power spectra from a series of experimental measurements, which are used in engineering practice for the accurate stochastic simulation of random physical
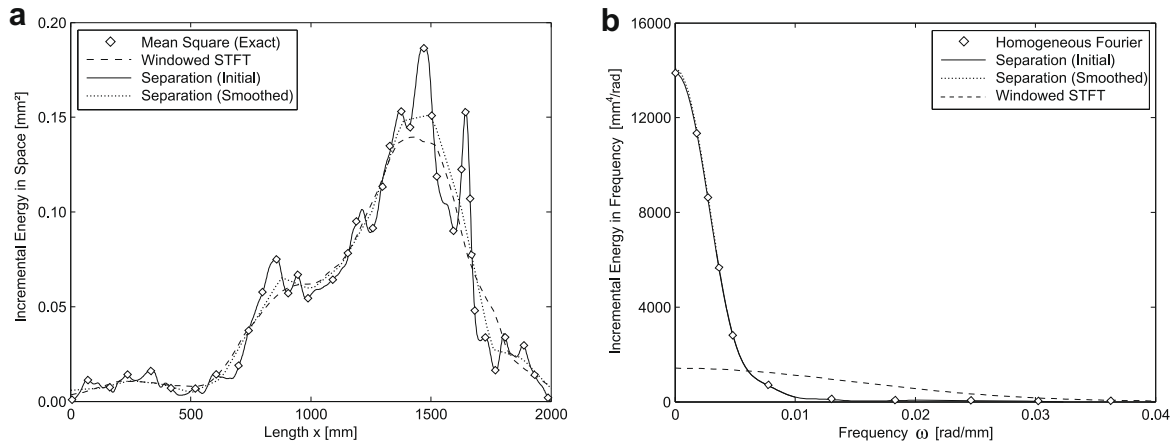
Fig. 19. Marginal densities (incremental energies) for STFT and method of separation based estimates of the imperfection example: (a) marginal density in space (mean square); and (b) marginal density in frequency.

phenomena by spectral representation. First, established evolutionary spectrum estimation techniques based on the short-time Fourier, the harmonic wavelet and the Wigner–Ville transforms have been briefly reviewed. Second, a method for the estimation of separable power spectra has been introduced, whose mathematical derivation directly implements the physical interpretation of the power spectrum as the distribution of the total energy over the space-frequency domain. For the estimation of the separable Kanai–Tajimi benchmark spectrum, the so-called method of separation has been confirmed to be more accurate in terms of surface regularity, space-frequency localization and stochastic convergence than each of the established techniques. The assumption of spectral separability, however, limits the method of separation to cases, where input samples do not or only slightly vary in frequency bandwidth along their length. Behind this background, it has been demonstrated that the constraint of spectral separability can be bypassed for a class of non-separable spectra, which can be partitioned into sub-regions of several separable sub-spectra.

The performance of the STFT, wavelet and Wigner–Ville based techniques and the proposed method of separation has been finally examined in the presence of strong narrow-bandedness and simultaneous spatial evolution on the basis of a practical example from imperfection modeling in structures. It has been shown that none of the established space-frequency analysis techniques is able to provide accurate evolutionary estimation results, which are suitable to be applied in the framework of spectral representation. In contrast to the established techniques, the method of separation has been demonstrated to yield good localization in space and frequency even in the presence of strong narrow-bandedness. In particular, it guarantees optimum frequency resolution, since the involved Fourier transforms take into account the complete available length of the measurements. The evaluation of marginal densities and the comparison of simulated imperfection samples with the experimental measurements could confirm the advantages of the method of separation in the case of strongly narrow-band input samples.

Acknowledgements

References

[1] J. Argyris, M. Papadrakakis, G. Stefanou, Stochastic finite element analysis of shells, Comput. Methods Appl. Mech. Engrg. 191 (2002) 4781–4804.
[2] R. Carmona, W.J. Hwang, B. Torresani, Practical Time-Frequency Analysis, Academic Press, New York, 1998.
[3] L. Cohen, Time-Frequency Analysis, Prentice-Hall, Upper Saddle River, NJ, 1995.
[4] J.P. Conte, B.F. Peng, Fully nonstationary analytical earthquake ground-motion model, J. Engrg. Mech. ASCE 123 (1997) 15–24.
[5] I. Daubechies, Ten Lectures on Wavelets, SIAM, Philadelphia, PA, 1992.
[6] G. Deodatis, P.D. Spanos (Eds.), Computational Stochastic Mechanics, in: Proceedings of the Fifth International Conference on Computing Stochastic Mechanics (CSM-5), IOS Press, Amsterdam, 2006.
[7] I. Elishakoff, Uncertain buckling: its past, present and future, Int. J. Solids Struct. 37 (2000) 6869–6889.
[8] R. Ghanem, P.D. Spanos, Stochastic Finite Elements: A Spectral Approach, Dover Publications, New York, 2003.
[9] M. Grigoriu, On the spectral representation method in simulation, Prob. Engrg. Mech. 8 (1993) 75–90.
[10] M. Grigoriu, Simulation of stationary non-Gaussian translation processes, J. Engrg. Mech. ASCE 124 (2) (1998) 121–126.
[11] A.S. Hasham, K.J.R. Rasmussen, Member Capacity of Thin-walled I-sections in Combined Compression and Major Axis Bending, Research Report No. R746, School of Civil Engineering, University of Sydney, 1997.
[12] J. Liang, S.R. Chaudhuri, M. Shinozuka, Simulation of non-stationary stochastic processes by spectral representation, J. Engrg. Mech. ASCE 133 (2007) 616–627.
[13] Y.K. Lin, Y. Yong, Evolutionary Kanai–Tajimi earthquake models, J. Engrg. Mech. ASCE 113 (1987) 1119–1137.
[14] R.G. Lyons, Understanding Digital Signal Processing, Prentice-Hall, Upper Saddle River, NJ, 2004.
[15] S. Mallat, A Wavelet Tour of Signal Processing, Academic Press, London, 1999.
[16] G. Manolis, P.K. Koliopoulos, Stochastic Structural Dynamics in Earthquake Engineering, WIT Press, Southampton, 2001.
[17] W. Martin, P. Flandrin, Wigner–Ville spectral analysis of non-stationary processes, IEEE Trans. Acoust., Speech Signal Process. 33 (6) (1985) 1461–1470.
[18] D.E. Newland, An Introduction to Random Vibrations, Spectral and Wavelet Analysis, Wiley, New York, 1993.
[19] D.E. Newland, Wavelet analysis of vibration, part I: theory, J. Vib. Acoust. 116 (1994) 409–416.
[20] D.E. Newland, Wavelet analysis of vibration, part II: wavelet maps, J. Vib. Acoust. 116 (1994) 417–425.
[21] D.E. Newland, Ridge and phase identification in the frequency analysis of transient signals by harmonic wavelets, J. Vib. Acoust. 121 (1999) 149–155.
[22] A.V. Oppenheim, R.W. Schafer, J.R. Buck, Discrete-Time Signal Processing, Prentice-Hall, Upper Saddle River, NJ, 1998.
[23] V. Papadopoulos, M. Papadrakakis, Finite element analysis of cylindrical panels with random initial imperfections, J. Engrg. Mech. ASCE 130 (2004) 867–876.
[24] V. Papadopoulos, M. Papadrakakis, The effect of material and thickness variability on the buckling load of shells with random initial imperfections, Comput. Methods Appl. Mech. Engrg. 194 (2005) 1405–1426.
[25] V. Papadopoulos, P. Iglesis, The effect of non-uniformity of axial loading on the buckling behaviour of shells with random imperfections, Int. J. Solids Struct. 44 (2007) 6299–6317.

[26] V. Papadopoulos, D.C. Charmpis, M. Papadrakakis, A computationally efficient method for the buckling analysis of shells with stochastic imperfections, Comput. Mech. 43 (2008) 687–700.

[27] A. Papoulis, S.U. Pillai, Probability, Random Variables and Stochastic Processes, McGraw-Hill, New York, 2002.

[28] E. Parzen, Stochastic Processes, SIAM, Philadelphia, PA, 1999.

[29] M. Pinsky, Introduction to Fourier Analysis and Wavelets, American Mathematical Society, Providence, RI, 2009.

[30] M.B. Priestley, Spectral Analysis and Time Series, Academic Press, London, 1981.

[31] M.B. Priestley, Nonlinear and Non-Stationary Time Series Analysis, Academic Press, London, 1988.

[32] C.A. Schenk, G.I. Schuëller, Buckling analysis of cylindrical shells with random geometric imperfections, Int. J. Non-Linear Mech. 38 (2003) 1119–1132.

[33] C.A. Schenk, G.I. Schuëller, Uncertainty assessment of large finite element systems, Lecture Notes in Applied and Computational Mechanics, vol. 24, Springer, Berlin, 2005.

[34] C.A. Schenk, G.I. Schuëller, Buckling analysis of cylindrical shells with cutouts including random boundary and geometric imperfections, Comput. Methods Appl. Mech. Engrg. 196 (2007) 3424–3434.

[35] M. Shinozuka, G. Deodatis, Simulation of stochastic processes by spectral representation, Appl. Mech. Rev. ASME 44 (1991) 191–203.

[36] M. Shinozuka, G. Deodatis, Simulation of multi-dimensional Gaussian stochastic fields by spectral representation, Appl. Mech. Rev. ASME 49 (1996) 29–53.

[37] P.D. Spanos, J. Tezcan, P. Tratskas, Stochastic processes evolutionary spectrum estimation via harmonic wavelets, Comput. Methods Appl. Mech. Engrg. 194 (2005) 1367–1383.

[38] G. Stefanou, M. Papadrakakis, Stochastic finite element analysis of shells with combined random material and geometric properties, Comput. Methods Appl. Mech. Engrg. 193 (2004) 139–160.

[39] G. Stefanou, M. Papadrakakis, Assessment of spectral representation and Karhunen–Loève expansion methods for the simulation of Gaussian stochastic fields, Comput. Methods Appl. Mech. Engrg. 196 (2007) 2465–2477.

[40] G. Stefanou, The stochastic finite element method: past, present and future, Comput. Methods Appl. Mech. Engrg. 198 (2009) 1031–1051.

[41] E. Stein, R. Shakarchi, Fourier Analysis: An Introduction, Princeton University Press, NJ, 2003.

[42] B. Sudret, A. Der Kiureghian, Stochastic Finite Element Methods and Reliability: A State-of-the-Art Report, Report No. UCB/SEMM-2000/08, University of California at Berkeley, 2000.

[43] P. Tratskas, P.D. Spanos, Linear multi-degree-of-freedom stochastic response by using the wavelet transform, J. Appl. Mech. ASME 70 (5) (2003) 724–731.

[44] E. Vanmarcke, Random Fields: Analysis and Synthesis, MIT Press, Cambridge, MA, 1983.